

A catapult action for rapid limb protraction

Energy bursts from a horse's elastic biceps muscles provide power for a flat-out gallop.

Fast runners must be able to protract their limbs quickly in order to prepare for the next stance phase^{1–3}. This is particularly challenging for large animals as their limbs are long⁴ and their muscles contract slowly and have a low power output^{5,6}. Here we show that horses cannot achieve the high power output required for rapid limb protraction by simple muscle contraction and that they instead deploy an elastic biceps muscle to store and then release bursts of energy — this muscle's catapult action has an output that is comparable to over 100 times its mass of non-elastic muscle. Although grasshoppers and fleas are known to rely on a similar catapult mechanism for rapid acceleration^{7,8}, to our knowledge this has not been demonstrated before in larger animals.

The legs of large cursorial animals function like pogo sticks, storing and returning energy during running gaits. This is a spring–mass system, so energy storage and return occupy similar periods of time^{7,9}. In a catapult, energy is stored slowly with a large force but is released quickly to accelerate a small mass^{7,10}. This mechanism, however, requires a more sophisticated lever, or cam system, to exert sufficient force on the spring and then release it^{7,10}. Such a system exists in the horse (Fig. 1) — the forward movement of the trunk and the orientation of the ground–reaction force (GRF) during stance stretches the biceps muscle while the carpus is locked in extension; in late stance, the carpus buckles and releases the leg.

At 50% of stance (Fig. 2a), the GRF is flexing the shoulder joint (resisted by the biceps), flexing the elbow (resisted by the triceps and digital flexor muscles) and extending the metacarpophalangeal joint (resisted by the digital flexors and suspensory ligament). At 90% of stance (Fig. 2a), the GRF has moved further behind the shoulder and is now also behind the elbow joint. The GRF is therefore further flexing the shoulder and extending the elbow, both of which stretch the biceps.

Through stance, the carpus is extended by the GRF and the tendinous link of lacertus fibrosis/extensor carpi radialis, and is flexed by the digital flexors and palmar carpal ligament. When the GRF approaches the neutral axis of the carpal joint, it no longer balances the digital flexors' moment (this occurs at around 90% of stance). The carpus then buckles forwards, destabilizing the limb and releasing the catapult. The GRF and the digital flexors subsequently fold the collapsed joint and the limb is

accelerated forwards by recoil of the biceps. At 101% of stance (Fig. 2a), the biceps muscle is flexing the elbow and extending the shoulder.

We used force-plate and motion analysis to work out the limb–joint angles and GRF moment at the shoulder of thoroughbred horses during trotting at 3 m s⁻¹ (n = 16). We determined biceps arm moment at the elbow and shoulder joints by radiography and dissection; tendon paths were roughly circular and were therefore assumed to be so. Eighty per cent of shoulder extensor moment was attributed to biceps and 20% to supraspinatus (apportioned from muscle architecture¹¹). Biceps length peaked at 91% of stance with a force of 11.4 kilonewtons (kN), and 74 joules (J) of elastic energy was stored. The biceps muscle has a substantial internal tendon (cross-sectional area, 200 mm²) which is parallel with two short-fibred (6 and 18 mm, respectively) pennate muscle heads¹².

Figure 2b shows the force–length relationship measured for biceps *in vitro* (n = 7) and *in vivo*. The similarity of the plots indicates that the muscle's properties *in vivo* are mainly passive. During galloping on a treadmill at 12 m s⁻¹, maximum biceps length was 12 mm greater than in trotting (at 100% of stance). Extrapolation of the curves shown in Fig. 2b by 12 mm gives a peak internal tendon strain of 7.5%, a force of 19.8 kN, and an elastic-energy storage of 261 J.



Figure 1 Good going: horses stretch and release their biceps in a gallop, creating 100 times the energy output of non-elastic muscle.

The energy released after the foot leaves the ground ('foot-off') was determined from biceps length and from the results shown in Fig. 2b, assuming that muscle fibres are isometric⁹ and that energy loss due to hysteresis is 7% (ref. 7). The sum of the kinetic and potential energy of the limb segments below the elbow (relative to the horse's centre of mass and segment height at foot-off, respectively) mirrored the biceps' elastic energy release, peaking at 33 J in a trot (Fig. 2c) and 120 J in a gallop. Some elastic energy was released before foot-off (Fig. 2b), and some energy accelerated the scapular and humeral segments and extrinsic muscle tissue.

The kinetic and potential energy of the limb continued to increase, but more slowly, after biceps energy/force had dropped to zero. This may indicate a shortening of the contractile component as it unloaded

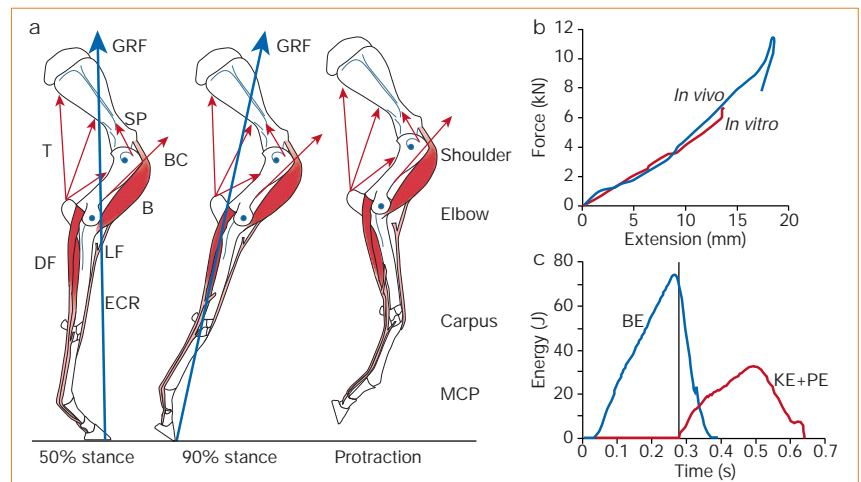


Figure 2 Mechanics of equine limb protraction. **a**, Equine forelimb at 50%, 90% and 101% (protraction) of stance, taken from our motion-analysis data. Biceps (B), brachiocephalicus (BC), supraspinatus (SP), triceps (T), lacertus fibrosis (LF), extensor carpi radialis (ECR) and digital flexor (DF) muscles are indicated. GRF, orientation of the ground–reaction force vector. MCP, metacarpophalangeal joint. **b**, Force–extension relationship for biceps *in vivo* in a trot (n = 16) and during tensile testing *in vitro* (n = 7). *In vivo* plot shows unloading as carpus and elbow flex before the foot is raised. **c**, Energetics of limb protraction. The foot makes contact at time zero and leaves the ground at the time indicated by the vertical line. Blue curve (BE) represents the elastic energy stored in the biceps through the gait cycle; red curve shows the sum of the kinetic and potential energy (KE + PE) of the radial, metacarpal and digital segments after foot-off.

(a common phenomenon) and/or work by the brachiocephalicus muscle. We devised a five-segment computer simulation of the equine limb that had biceps represented by a spring ($k = 700 \text{ kN m}^{-1}$) and recorded the joint angles at foot-off. The joint angular acceleration curves and segment trajectories generated by the simulation were very similar to those that we observed *in vivo* (see supplementary information).

The biceps released 243 J in 0.11 s in a gallop (2,200 W), which equates to a muscle with a peak power output of roughly 4,400 W (ref. 10). Equine muscle has a peak power output of about 90 W kg^{-1} ($V_{\text{max}} = 3.0$ lengths per second^{5,6}; $F_{\text{max}} = 0.3 \text{ MPa}$ (refs 5, 9, 10); $a/P_0 = 2.5$ (ref. 5)). A horse would therefore require 50 kg of non-elastic muscle to achieve the same power output as a 0.4-kg biceps muscle. The peak power output of brachiocephalicus (identified as the main forelimb protractor¹³) would be only 220 W. The catapult mechanism is therefore essential for rapid protraction of the equine limb, and it is likely that similar mechanisms exist in other animals.

Alan M. Wilson*†, Johanna C. Watson*,

Glen A. Lichtwark†

*Structure and Motion Laboratory, Department of Veterinary Basic Sciences, The Royal Veterinary College, Hatfield, Herts AL9 7TA, UK
e-mail: awilson@rvc.ac.uk

†Institute of Human Performance, University College London, Stanmore, Middlesex HA7 4LP, UK

1. Weyand, P. G., Sternlight, D. B., Bellizzi, M. J. & Wright, S. *J. Appl. Physiol.* **89**, 1991–1999 (2000).
2. Pratt, G. W. & O'Connor, J. T. *Am. J. Vet. Res.* **39**, 249–253 (1978).
3. Hutchinson, J. R. & Garcia, M. *Nature* **415**, 1018–1021 (2002).
4. Schmidt-Nielsen, K. *Scaling: Why is Animal Size so Important?* (Cambridge Univ. Press, Cambridge, 1984).
5. Woledge, R. C., Curtin, N. A. & Homsher, E. *Monogr. Physiol. Soc.* **41** (Academic, London, 1985).
6. Rome, L. C., Sosnicki, A. A. & Goble, D. O. *J. Physiol.* **431**, 173–185 (1990).
7. Alexander, R. McN. *Elastic Mechanisms in Animal Movement* (Cambridge Univ. Press, Cambridge, 1988).
8. Bennet Clark, H. C. *J. Exp. Biol.* **63**, 53–83 (1975).
9. Biewener, A. A. & Roberts, T. J. *Ex. Sport Sci. Rev.* **28**, 99–107 (2000).
10. Peplowski, M. M. & Marsh, R. L. *J. Exp. Biol.* **200**, 2861–2870 (1997).
11. Biewener, A. A. *Comp. Biochem. Physiol. B* **120**, 73–87 (1998).
12. Hermanson, J. W. & Hurley, K. J. *Acta Anat.* **137**, 146–156 (1990).
13. Dyce, K. M., Sack, W. O. & Wensing, C. J. G. (eds) *Textbook of Veterinary Anatomy* 2nd edn, 542–575 (Saunders, London, 1987).

Supplementary information accompanies this communication on Nature's website.

Competing financial interests: declared none.

Outer planets

Origins of atmospheric zonal winds

The origin of the strong zonal (east–west) jets at cloud-top level in the atmospheres of Jupiter and Saturn¹ is something of a mystery^{2,3}. Using an idealized two-dimensional, deep-turbulence model applied to a rapidly rotating planetary interior that is mixed by thermal convection, we are able to simulate the atmospheric multiple jets of these giant

planets, and show that deep origins may explain one of their distinguishing features — the prograde (westerly) equatorial jets.

This feature cannot be reproduced in conventional shallow-atmosphere models. A set of idealized simulations of single fluid-layer flows on a rotating sphere, starting from a random initial condition⁴, explains both the magnitude and the number of jets well, but has an important defect in that it produces retrograde (easterly) jets at the equator. The reason for this defect is that turbulent horizontal mixing of the planetary rotational vorticity, which has opposite signs in the two hemispheres, gives rise to a slower (retrograde) atmospheric rotation than the planetary value over the equator. The sign of the parameter β , defined as the rate of change of the Coriolis parameter with latitude, dictates the sign of the jets (see equation (2.4) in ref. 5) by the conservation of potential vorticity⁶, which measures the total strength of the atmospheric vorticity tube, in the course of this mixing process⁷.

The atmospheres of Jupiter and Saturn are much deeper than Earth's atmosphere, however, making possible completely different dynamics^{8–10} in which the flows are deep, extending from one hemisphere to another. These flows are homogeneous

in the direction of the axis of planetary rotation when the planetary interior is well mixed by thermal convection⁸. A single fluid layer, confined within the planetary sphere, therefore describes these deep flows¹⁰.

Analogous dynamics that conserve a potential vorticity govern this system, which is defined in terms of the deep fluid tubes parallel to the axis of planetary rotation. The resulting β , which now measures the rate of change in the length of fluid tubes with latitude, takes the opposite sign^{2,9}. Consequently, the equatorial jet also has an opposite sign, as has been observed. Lateral transport of stronger potential vorticity, owing to longer fluid tubes, from higher latitudes to the equator, gives rise to faster (prograde) rotation.

To demonstrate this, we run the model, assuming constant density and no convective buoyancy forcing, for a long period, starting from a random state with wind variance of 100 m s^{-1} and 200 m s^{-1} for Jupiter and Saturn, respectively. These magnitudes are comparable to those observed^{1,4}. In both cases, we obtain the prograde equatorial jets of the correct width and magnitude, and also with an indication of multiple jets (Fig. 1).

Another attractive feature of our 'deep' model is that the magnitude of β values is greater, which relaxes the wind-shear stability criterion⁹ and opens the way for obtaining steeper high-latitude jets, in accordance with observations. This is another feature that conventional shallow models can reproduce only with difficulty. Inclusion of a convective buoyancy force⁸ would give rise to steeper jets in our deep model.

Jun-Ichi Yano*, Olivier Talagrand†, Pierre Drossart‡

*Laboratoire de Météorologie Dynamique, École Polytechnique, F-91128 Palaiseau, France
e-mail: yano@cnrm.meteo.fr

†LMD, Ecole Normale Supérieure, F-75231 Paris, France

‡LESIA (CNRS-FRE2461), Observatoire de Paris, F-92125 Meudon, France

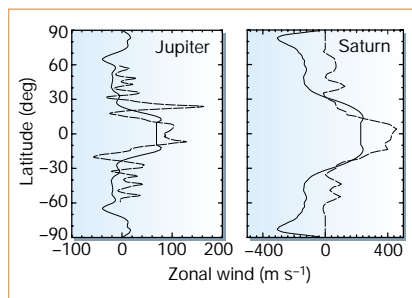


Figure 1 Simulated zonal winds (solid lines) and actual observations (dashed lines) for Jupiter and Saturn, after 300 and 100 planetary rotations, respectively, from an initial random state. Here, for numerical stability, spherical geometry is replaced by a cylindrical wall parallel to the axis of planetary rotation at 99% of the planetary radius, which intersects with the planetary surface at $\pm 8.1^\circ$ latitude. The plot assumes that homogeneous winds on this cylindrical wall are directly observed at the cloud tops of the lower latitudes. Full modelling details are available from the authors.

1. Ingersoll, A. P. *Science* **248**, 308–315 (1990).
 2. Yano, J.-I. *Chaos* **4**, 287–297 (1994).
 3. Ingersoll, A. P., Gierasch, P. J., Banfield, D., Vasavada, A. R. & Galileo Imaging Team *Nature* **403**, 630–632 (2000).
 4. Cho, J. Y.-K. & Polvani, L. M. *Science* **273**, 335–337 (1996).
 5. Yano, J.-I. & Flierl, G. R. *Dyn. Atmos. Ocean* **16**, 439–472 (1992).
 6. Pedlosky, J. *Geophysical Fluid Dynamics* 2nd edn (Springer, New York, 1987).
 7. Rhines, P. B. & Young, W. R. *J. Fluid Mech.* **122**, 347–367 (1982).
 8. Busse, F. H. *Icarus* **29**, 255–260 (1976).
 9. Ingersoll, A. P. & Pollard, D. *Icarus* **52**, 62–80 (1982).
 10. Yano, J.-I. & Flierl, G. R. *Ann. Geophysicae* **12**, 1–18 (1994).
- Competing financial interests: declared none.

brief communications is intended to provide a forum for both brief, topical reports of general scientific interest and technical discussion of recently published material of particular interest to non-specialist readers. Priority will be given to contributions that have fewer than 500 words, 10 references and only one figure. Detailed guidelines are available on Nature's website (www.nature.com) or on request from nature@nature.com/nature.